RESEARCH ARTICLE

Redox behavior of In–O–Ti interface for selective hydrogenation of CO_2 to CO in doped In–TiO_2 catalyst

Nazmul H. MD. Dostagir, [a] Atsushi Fukuoka,* [a] Abhijit Shrotri*[a]

[a] Dr. N. H. MD. Dostagir, Prof. A. Fukuoka, Dr. A. Shrotri
Institute for Catalysis
Hokkaido University
Kita 21 Nishi 10, Kita-ku, Sapporo, Hokkaido 001-0021, Japan
E-mail: ashrotri@cat.hokudai.ac.jp, fukuoka@cat.hokudai.ac.jp

Supporting information for this article is given via a link at the end of the document.

Abstract: In CO_2 hydrogenation reaction, selective synthesis of CO at low temperature and high pressure is needed to integrate the reverse water gas shift reaction with Fischer-Tropsch synthesis. Here, we show that a mixed oxide catalyst prepared by doping indium (In) into TiO_2 produces CO with the formation rate of 22 μmol g^{-1} s^{-1}. The CO selectivity was more than 99% at 350 °C and 3 MPa pressure. Moreover, the catalyst was durable for over 100 h on stream. During reaction the interfacial In^{3+}–O–Ti^{4+} sites were first reduced in presence of H_2 and then oxidized back with CO_2 producing CO. Because of the redox mechanism, methanol and methane formation was limited. This study shows the development of a promotor free oxide catalyst for CO_2 hydrogenation and the importance of the redox property at the oxidic interface for selective hydrogenation of CO_2 to CO under unfavorable conditions.

Introduction

Hydrogenation of CO_2 is an attractive way to produce chemicals and fuels without using fossil resources. Production of CO by partial reduction of CO_2, also known as reverse water gas shift (RWGS) reaction (Equation 1), is of interest because the conversion of CO to hydrocarbon fuels and useful chemicals through Fischer-Tropsch synthesis (FTS) is already industrially established.[1–5] Usual operating condition for RWGS is above 500 °C and atmospheric pressure.[4] Under these conditions several catalysts have been reported for RWGS that achieve high CO yield.[6,7] However, to effectively couple the two processes, the condition of RWGS reaction should match the subsequent FTS reaction, which is conducted at less than 400 °C and under a pressure of 1-3 MPa.[8] At lower temperature and high pressure CO selectivity reduces because RWGS reaction is endothermic in nature and formation of methanol and methane is favored.[9] Therefore, it is important to develop efficient catalysts that are selective for CO formation under unfavorable conditions of low temperature and high pressure to match with the subsequent FTS processes.

$$CO_2 + H_2 \rightarrow CO + H_2O \qquad (1)$$

Noble metal-based catalysts containing Pt has been reported for RGWS at low temperature. For example, Pt/mullite and $PtCo/TiO_2$ catalysts showed high selectivity of CO with activity of 12.5 and 11.4 μmol g^{-1} s^{-1}, respectively.[10,11] Single atom Pt catalysts are used to increase the atom efficiency of Pt metal. However, cost of noble metals is prohibitive and they are prone to deactivation due to aggregation of metal sites.[12–14] Non-noble metal catalysts containing Ni or Co tend to produce CH_4 and higher hydrocarbons instead of CO.[15–17] Cu based catalysts are the exception because of their high activity for RWGS at low temperatures. In particular, Cu supported on reducible supports, especially CeO_2 catalysts, are comparable to noble metals based catalyst for RWGS.[18–24] Cu supported over hollow nanosphere of CeO_2 containing high density of oxygen vacancy produced 55 μmol g^{-1} s^{-1} of CO at 350 °C.[23] Similarly, Cu/CeO_2 catalyst derived from pyrolysis of a copper containing metal organic framework (MOF), produced CO at a rate of ca. 9.5 μmol g^{-1} s^{-1} at 400 °C. Despite the excellent activity achieved by supported Cu catalysts they are prone to deactivation. For example, MOF derived Cu/CeO_2 catalyst lost 25% of activity within the first 24 h.[18] The cause of deactivation in Cu catalysts is aggregation of Cu metal particles.[25,26] Mixed metal oxide catalysts are considered as promising alternatives because they are stable under CO_2 hydrogenation condition. Oxygen vacancy on the interface of mixed oxide adsorbs and activates CO_2. However, the interfacial sites promote deep hydrogenation of CO_2 to CH_3OH and CH_4 because the oxophilic vacancy tends to stabilize the reaction intermediates such as formate and methoxy species.[27,28]

In this work, we report the synthesis of an In-TiO_2 mixed oxide catalyst for RWGS reaction by doping In in TiO_2. In atoms were atomically dispersed throughout the anatase TiO_2 framework. In–O–Ti interfacial site was partially reduced under CO_2 hydrogenation condition and acted as a redox center for CO_2 hydrogenation to CO. The reducibility and oxidizability of both In and Ti at the interfacial site facilitated the redox mechanism leading to high activity and CO selectivity. Indium doped TiO_2 produced CO with >99% selectivity with high yield. CO selectivity did not reduce even under high pressure.

Results and Discussion

Catalyst synthesis and characterization

Initially, two types of catalyst with interfacial In–O–Ti sites were synthesized by doping indium in titania (In–TiO_2) and by doping titanium in In_2O_3 (Ti–In_2O_3). Both catalysts were prepared by mixing In and Ti precursors with citric acid to form a sol that was dried and calcined to obtain the doped oxides. The atomic ratio of In:Ti in In–TiO_2 was 1:28 (corresponding to 5 wt.% In loading) and the atomic ratio of Ti:In in Ti-In_2O_3 was also 1:28. Doping of In and Ti had little influence on the physical structure of their parent bulk oxides. Titania showed anatase crystal phase in In–TiO_2, which was same as undoped TiO_2 that was also prepared by the sol gel method (Figure 1a). Conversely, In_2O_3 exhibited cubic phase in Ti–In_2O_3, same as undoped In_2O_3. No crystal peak of dopant oxides was observed in both the doped catalysts. Doped oxides showed shifting of XRD peak as compared to their undoped analogues (Figure S1). When In was doped into TiO_2, the interplanar distance increases because In^{3+} (0.8 Å) is larger than Ti^{4+} (0.6 Å). As a result, 2θ value of In-TiO_2 XRD patterns decreased as compared to undoped TiO_2 (Figure S1a). Due to the same reason, the XRD patterns of Ti-In_2O_3 shifted towards higher 2θ value as compared to undoped In_2O_3 (Figure S1b). The doped catalysts also showed similar N_2 adsorption isotherms and surface area as compared to their undoped counterpart oxides (Figure 1b and Table S1).

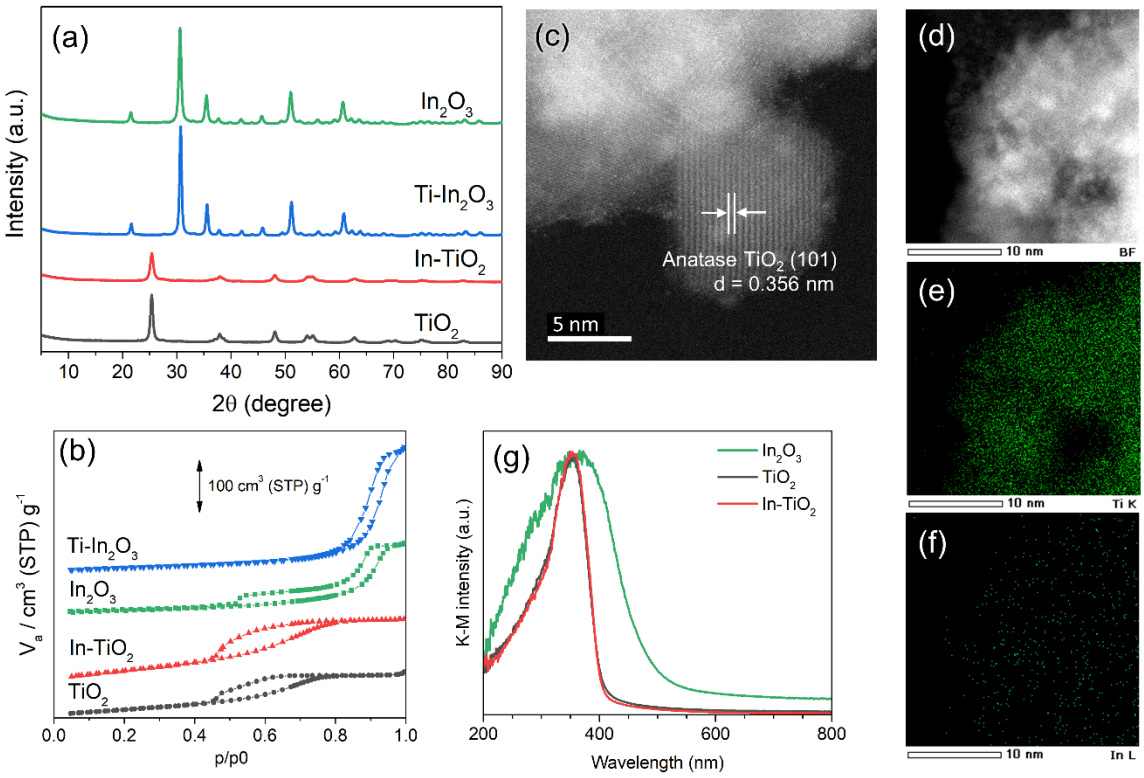

Figure 1. (a) XRD pattern of In–TiO_2 and Ti–In_2O_3 doped catalyst along with undoped single oxides. (b) N_2 adsorption isotherms of In-TiO_2, Ti-In_2O_3 and undoped analogues. (c) HAADF-STEM image of In-TiO_2 showing anatase crystal structure of TiO_2. EDX elemental mapping of the selected region (d) showing the homogeneous distribution of (e) Ti and (f) In. (g) Diffuse reflectance UV-Vis absorption spectra of In-TiO_2 compared with undoped TiO_2 and In_2O_3.

Further characterization showed that the dopants were highly dispersed without agglomeration. In the high-angle annular dark field scanning transmission electron microscopy (HAADF-STEM) analysis of In–TiO_2 (Figure 1c), only anatase titania phase was observed. In was highly dispersed in TiO_2 as seen in elemental mapping by energy dispersive X-ray (EDX) analysis (Figure 1d-f). Also, the results from diffuse reflectance UV-Vis absorption spectroscopy show that In was atomically dispersed in In–TiO_2. In the UV-Vis spectra absorption peak at 340 nm was observed corresponding to the electronic transition from valence band to conductance band for anatase titania (Figure 1g).[29] Features indicating formation of In_2O_3 crystals, such as electronic transition from valence band to conductance band and broadening until 600 nm, were not present.[30]

Similar to In-TiO_2, HAADF-STEM image of Ti–In_2O_3 (Figure S2a) showed cubic In_2O_3 and TiO_2 was not observed. Highly dispersed Ti was observed in the elemental mapping analysis (Figure S2b-d). In the UV-Vis analysis, the absorption peak position for Ti–In_2O_3 was shifted towards lower wavenumber as compared to undoped In_2O_3 due to the doping of Ti in In_2O_3 (Figure S3).[31] These results show that mixed oxide of In–TiO_2 and Ti–In_2O_3 were formed and the dopant was dispersed in the parent oxide without formation of agglomerated particles.

Catalytic activity

After confirming the formation of mixed oxide containing interfacial In–O–Ti sites, these catalysts were tested for CO_2 hydrogenation reaction in a fixed bed flow reactor at 300 °C, 3 MPa, 30,000 mL h^{-1} g_{cat}^{-1}, H_2:CO_2 = 3:1. In the presence of In–TiO_2 catalyst, CO_2 conversion was 7.4% with CO selectivity of more than 99% with traces of CH_4 (Figure 2a). Undoped TiO_2 showed negligible CO_2 conversion of 0.1%. Therefore, doping indium in TiO_2 enhanced its activity for CO_2 hydrogenation while favoring CO as the only product. For Ti–In_2O_3 catalyst, CO selectivity was 70% along with 4.6% CO_2 conversion. In contrast, undoped In_2O_3 produced methanol as the primary product with a selectivity of 54% and CO_2 conversion of 4.4%. Because Ti–In_2O_3 and undoped In_2O_3 had similar surface area and they showed similar CO_2 conversion, the shift in selectivity from methanol to

CO was attributed to doping of Ti in In_2O_3. Therefore, presence of In–O–Ti interfacial site favored the formation of CO in Ti–In_2O_3 and In–TiO_2 catalysts.

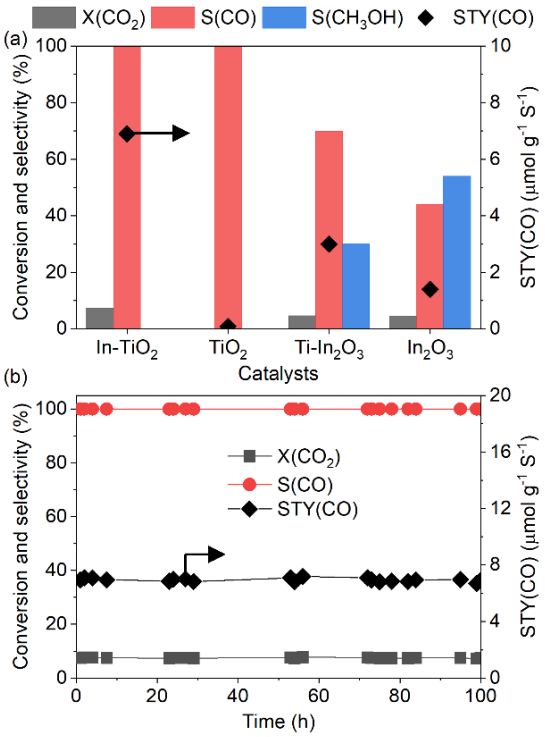

Figure 2. (a) Comparison of CO_2 hydrogenation activity of different catalysts. (b) Long term stability of In–TiO_2 during CO_2 hydrogenation. Reaction condition: 300 °C, 3 MPa, 30000 mL h^{-1} g^{-1}, H_2:CO_2 = 3:1.

Further optimization of reaction condition over In–TiO_2 showed that the selective formation of CO was independent of hydrogenation reaction condition. Increasing the temperature to 350 °C increased the CO_2 conversion from 7.4% to 19.5% without any change in CO selectivity (Table 1). Typically, CO selectivity in RWGS reaction is favored at high temperature and low pressure.[32–34] In contrast, CO selectivity was more than 99% over In–TiO_2 irrespective of change in pressure, temperature and space velocity. At 350 °C and 3 MPa, the CO space time yield (STY) was 18 μmol g^{-1} s^{-1}, which was comparable to that of noble metal-based catalysts under similar reaction condition (Table S2). At an SV of 60,000 the STY increased to 22 μmol g^{-1} s^{-1}. The catalyst was stable in long term reaction and did not show any loss in activity or selectivity after 100 h on stream (Figure 2b). Therefore, interfacial In–O–Ti sites formed on In–TiO_2 showed remarkable activity and stability for selectively converting CO_2 to CO over a wide range of reaction condition.

Table 1. Activity of In-TiO_2 catalyst at different reaction conditions.[a]

T (°C)	P (MPa)	SV (ml h^{-1} g^{-1})	CO_2 Conv. (%)	CO Sel. (%)	STY (μmol g^{-1} S^{-1})
300	0.1	30,000	1.0	100	0.98
300	3	30,000	7.4	>99	6.9
350	3	30,000	19.5	>99	18
350	3	60,000[b]	11.7	>99	22

[a]Catalyst: In-TiO_2 200 mg, H_2:CO_2 = 3:1.

[b]Catalyst amount was halved to 100 mg.

Mechanistic Clarification

After confirming the presence of interfacial In–O–Ti active site and its high activity for CO production, In–TiO_2 catalyst was further analyzed to ascertain the mechanism of CO formation and the role of surface interface. Doping of In increased the H_2 dissociation ability of catalysts at lower temperature (Figure 3a). Undoped TiO_2 showed little H_2 consumption below 550 °C during temperature programmed reduction (TPR) under H_2 flow. H_2 consumption in the temperature range of 250-400 °C was observed for In–TiO_2 catalyst, which was assigned to reduction of In–O–Ti interface.

Above 500 °C, surface indium atoms underwent complete reduction to form metal nanoparticles. This was evidenced by XRD of In-TiO_2 treated at 550 °C under H_2 (Figure S4). Above 700 °C anatase TiO_2 transformed to rutile phase. In the XRD spectrum of sample treated at 700 °C metallic In nanoparticle peak increased in size as In withing the bulk crystal also reduced during phase transition of TiO_2 (Figure S4).

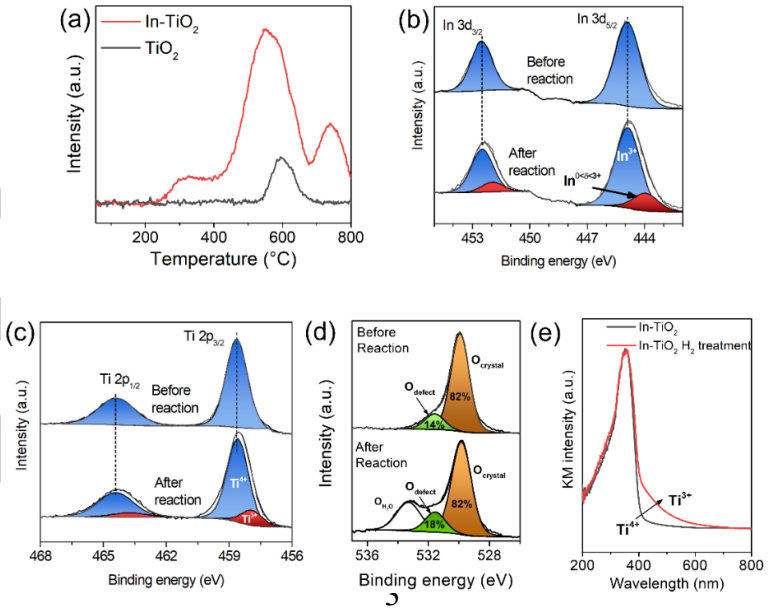

Figure 3. (a) H_2 TPR spectra of In–TiO_2 and undoped TiO_2. (b), (c), and (d) XPS spectra of In-TiO_2 catalyst before and after CO_2 hydrogenation for In 3d, Ti 2p and O 1s regions, respectively. (e) UV-Vis analysis for In-TiO_2 before and after treatment under H_2 atmosphere at 350 °C showing formation of Ti^{3+} species.

The partial reduction of In–O–Ti interfacial sites at low temperature (below 400 °C) was evident from ex-situ X-ray photoelectron spectroscopy (XPS) and UV-Vis analysis. In XPS analysis of In–TiO_2 catalyst after CO_2 hydrogenation reaction, a peak for partially reduced In species was present at 443.9 eV (Figure 3b).[35] Similarly, in the Ti 2p XPS spectra, presence of Ti^{3+} at 458 eV in the used catalyst was also observed (Figure 3c).[36,37] This suggests that during reaction, both In^{3+} and Ti^{4+} present at the interface were partially reduced. As a result, an increase in oxygen defects was observed in the O 1s XPS spectra from 14% to 18% (Figure 3d). In the UV-Vis spectrum for In–TiO_2 a broad shoulder appeared in the range of 400-700 nm after treating the catalyst under H_2 at 350 °C (Figure 3e). This shoulder was assigned to formation of Ti^{3+} species due to reduction of the metal oxide interface.[29,38] Similar shoulder did not appear when undoped TiO_2 was subjected to H_2 treatment (Figure S5). Therefore, In-O-Ti interface underwent reduction during the reaction to form $In^{0<\delta<3+}$-V_o-Ti^{3+}, where V_o denotes an oxygen vacancy.

Oxide catalysts bearing oxygen vacancies are known to strongly adsorb CO_2, which increases their catalytic activity.[39] Such CO_2 species, present in bent or carbonate form, undergo hydrogenation to form formate or carboxyl intermediate via associated mechanism. In a CO_2 temperature programmed desorption (TPD) these species desorb at temperatures above 300 °C.[39] However, TPD of CO_2 adsorbed over H_2 pretreated In–TiO_2 only exhibited CO_2 desorption peak at 120 °C assigned to physisorbed and weakly adsorbed CO_2 species (Figure S6a). There was negligible desorption of CO_2 above 300 C indicating absence of strongly adsorbed CO_2 species necessary for CO_2 conversion by associated mechanism. Investigation of adsorbed CO_2 species using diffuse reflectance infrared Fourier transform spectroscopy (DRIFTS) further confirmed that bicarbonate and carbonate species formed during room temperature adsorption of CO_2 disappeared before 250 °C and such species were not detected at 350 °C (Figure S6b). When the DRIFTS experiment was performed under in-situ conditions, intermediate species of RWGS reaction such as formate or carboxyl were not detected over In–TiO_2 catalyst and only peaks for gaseous CO were observed at 2172 and 2109 cm^{-1} (Figure S7).[40] Over In_2O_3, carboxyl and formate species are known to be the intermediates for methanol and CO formation through the association mechanism.[41] Therefore, the formation of CO without the presence of any intermediate indicated that CO might be produced via, redox mechanism (also called reverse Mars-van Krevelen mechanism), where H_2 reduces the In–O–Ti interface and CO_2 directly oxidizes the interface to produce CO.

To confirm the redox nature of mechanism, In–TiO_2 was first treated with H_2 at 300 °C for 15 min and then purged with Ar to remove the residual H_2 gas. Then a mixture of Ar and CO_2 was passed over the catalyst and the evolution of CO was recorded using a GC. CO evolution was observed for more than 20 min even in the absence of H_2 (Figure 4a). Repeating the reduction and oxidation cycle a second time gave identical result. In contrast, when undoped In_2O_3 catalyst was used, product evolution was poor (Figure S8). The redox cycle of In–TiO_2 catalyst was also observed ex-situ by UV-VIS spectroscopy after each reduction and oxidation cycle (Figure 4b). Formation of Ti^{3+} species was apparent after the first reduction step owing to the appearance of broad shoulder at 400-500 cm^{-1} (Figure 4b, spectra a and b)). After CO_2 treatment the intensity of the Ti^{3+} shoulder reduced in UV-Vis spectrum (Figure 4b, spectrum c). This phenomenon was reversible under repetitive reduction and oxidation cycles (Figure 4b, spectra c-e). Therefore, we conclude that In–TiO_2 catalyzed CO_2 reduction to CO through reverse Mars-van Krevelen mechanism, at the interface of In and Ti atoms.

Figure 4. (a) Rate of CO production over pre-reduced In–TiO_2 when flowing

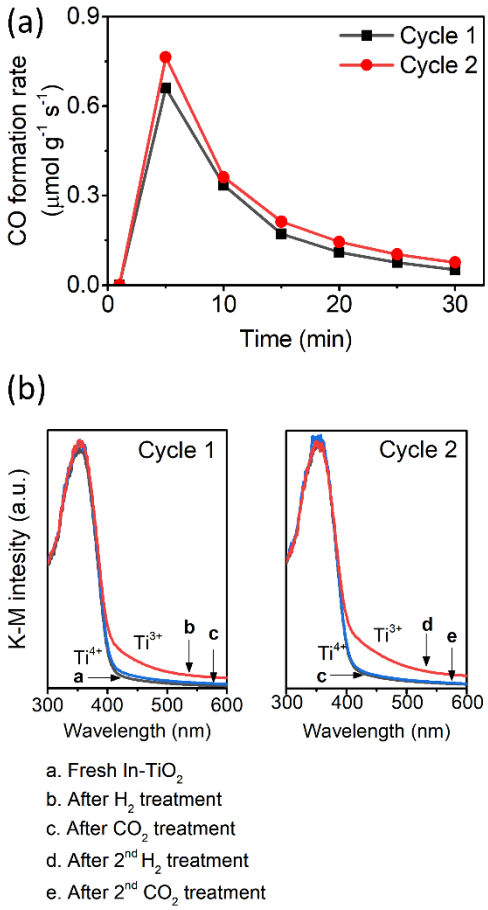

CO_2 in the absence of H_2 at 300 °C. For each cycle catalyst was first reduced with H_2 at 300 °C before flowing CO_2. (b) UV-Vis spectra of In–TiO_2 catalyst after successive treatment with H_2 and CO_2 showing transition between Ti^{4+} and Ti^{3+} species over the surface.

Scheme 1 depicts the mechanism for CO_2 hydrogenation over the surface of In–TiO_2. Catalyst characterization has shown that doping In in TiO_2 enhances reduction of the catalyst surface under the reaction condition. Formation of partially reduced In species and Ti^{3+} confirms the reduction of In^{3+}–O–Ti^{4+} interfacial site. Although the surface reduction generated oxygen vacancy, it did not cause chemisorption of CO_2 on the catalyst surface favorable for formate or carboxyl formation. Instead, the partially reduced In and Ti^{3+} at the interfacial site interacted with the O of CO_2 and they were oxidized by CO_2. The oxygen deficient site is replenished to recover In^{3+}–O–Ti^{4+} species and CO was produced and removed from the catalyst surface. Because intermediates were not formed during the reaction their subsequent hydrogenation to methane or methanol was less likely. Furthermore, owing to high dispersion of In species and lack of

metal nanoparticles, hydrogenation of CO to methane was suppressed. Consequently, high CO selectivity was maintained even at low temperature and high pressure, which are favorable for methane formation. The reversibility of the In–O–Ti interface for redox reaction without undergoing over reduction ensured the stability of the catalyst.

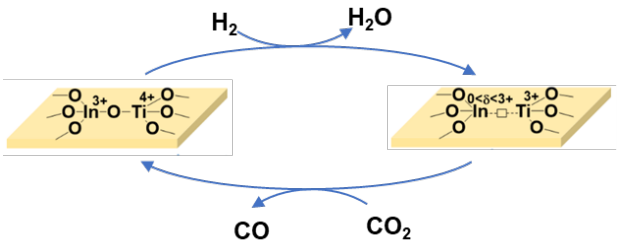

Scheme 1. Catalytic CO_2 hydrogenation to CO over In–TiO_2 catalyst through reverse Mars-van Krevelen pathway.

Conclusion

In summary, we show that doping of In into TiO_2 led to the formation of highly active and selective interfacial active site for the RWGS reaction. The activity of CO production over In–TiO_2 catalyst was comparable to noble metal-based catalysts. More than 99% selectivity of CO was obtained 350 °C and 3MPa pressure. Under the reaction condition, interfacial In^{3+}–O–Ti^{4+} site was first reduced in presence of H_2 to form $In^{0<\delta<3+}$-V_o-Ti^{3+} and then oxidized back with CO_2 producing CO. Consequently, the reaction proceeded through reverse Mars-van Krevelen mechanism. The formation of methane was suppressed because of lack of metal nanoparticles to catalyze hydrogenation of CO. As a result, RWGS reaction was possible at conditions similar to Fischer-Tropsch synthesis. The redox property at the interfacial site shown in this study can also be applied to reactions other than CO_2 hydrogenation and can help in the development of promoter free oxide catalysts for redox reactions.

Experimental Section

Catalyst preparation

Indium nitrate ($In(NO_3)_3{\cdot}3H_2O$), aqueous titanium chloride solution (aqueous solution of 20% $TiCl_3$ containing 5% HCl) and citric acid were purchased from Fujifilm Wako Pure Chemical Corporation. All catalysts were prepared using a sol-gel method in the presence of citric acid. A typical procedure to obtain In-TiO_2 catalysts is as follows: $In(NO_3)_3{\cdot}3H_2O$ (0.435 mmol) and $TiCl_3$ (12.5 mmol) solution were added to a beaker containing 60 mL of H_2O along with 20 mmol of citric acid. The beaker was placed on a hot plate maintained at 150 °C and stirred until a foaming gel was formed. The gel was then dried in an oven maintained at 150 °C for 5 h. The resulting composite was crushed and calcined at 500 °C for 3 h (ramp rate: 2 °C min^{-1}) to obtain the final catalyst. For Ti-In_2O_3, 0.453 mmol of $TiCl_3$ and 12.5 mmol of $In(NO_3)_3.3H_2O$ were used and same method was followed. Undoped oxides were prepared in the same manner without the presence of the dopant.

Catalyst Characterization

X-ray diffraction (XRD) pattern was measured with Rigaku MiniFlex using CuKα X-ray (λ = 1.54 Å) operating at 40 kV and 20 mA. N_2 adsorption isotherms were measured at −196 °C using a Belsorp mini analyzer. Prior to the adsorption, all samples were degassed under vacuum at 120 °C for 2 h. Surface area was calculated by using BET theory between the relative pressure range 0.05 to 0.35 in the N_2 adsorption isotherm. X-ray photoelectron spectroscopy (XPS) was performed with JEOL JPS-9010MC instrument. Charge correction was done by adjusting the carbon peak to 284.6 eV. STEM images were obtained in a JEOL JEM-ARM200F atomic resolution electron microscope at an acceleration voltage of 200 kV equipped with EDS detector EX-24221M1G5T. Temperature programmed reduction (TPR) of catalysts was carried out in presence of H_2-Ar mixture (H_2 = 5%) in a BELCAT II instrument equipped with a TCD detector. Prior to measurement, catalysts were pretreated at 200 °C for 1 hour under Ar flow. Measurements were done at a total flow rate of 50 mL min^{-1} with ramp rate of 10 °C min^{-1}. CO_2 TPD experiment was performed in the BELCAT II instrument equipped with BELMass gas mass spectrometer. Prior to measurement, the samples were pretreated under He at 200 °C for 60 min followed by CO_2 adsorption at room temperature for 30 min. After purging with He for 30 min TPD was performed with a ramp rate of 10 °C min^{-1}. DRIFTS experiments were done using a Perkin Elmer Spectrum 100 FTIR spectrometer equipped with MCT detector cooled with liquid N_2. The catalyst was first pretreated under He at 300 °C for 30 min. One spectrum of catalsyt was recorded as background under He before flowing reactant gases (H_2:CO_2 = 3). Final IR spectrum of the adsorbed species was obtained by subtracting the background spectrum of the catalyst. The UV-Vis analysis was carried out in a JASCO V-650 spectrophotometer. To check the redox property of the catalyst in the reactor, first the catalyst was reduced under H_2 for 15 min at 300 °C followed by the Ar flow to remove H_2 gas. Then the catalyst was treated with a mixture of Ar and CO_2 and the evolution of CO was recorded in GC-TCD. This whole procedure was repeated on the same catalyst bed to ensure the reproducibility of the redox process. The UV-Vis analysis of the redox process was done by treating the same batch of catalyst under different atmospheres and quickly analyzing the treated catalyst in the spectrophotometer. For comparison between different samples, peak intensities were normalized according to the primary peak intensity of undoped TiO_2.

Evaluation of catalytic activity

Catalytic activity for CO_2 hydrogenation was evaluated in a stainless-steel fixed bed flow reactor system. Products were analyzed using an online GC (Shimadzu, GC 8A) equipped with two columns – Porapak Q and Molecular Sieve and a TCD detector. Gas line from the outlet of the reactor to the inlet of the GC was heated at 150 °C to prevent condensation. Typically, 200 mg of catalyst was loaded into the reactor and held in place by quartz wool. A thermocouple was inserted into the reactor to measure catalyst bed temperature. The reactor was pressurized to reaction condition using a mixture of H_2 and CO_2 having the ratio H_2:CO_2 = 3:1. After the system pressure was stable, reactor temperature was increased to desired value. Total flow rate was 100 mL min^{-1} to maintain space velocity at 30,000 mL h^{-1} g^{-1}. Reactions at space velocity higher than 30,000 mL h^{-1} g^{-1} were carried out by reducing the amount of catalyst.

CO_2 conversion, selectivity of CO and CH_3OH and space time yield (STY) of CH_3OH were calculated using the following equations.

CO_2 conversion (equation 2):

$$X_{(CO_2)} = \left(\frac{nCO_{out} + nCH_3OH_{out} + nCH_{4\,out}}{nCO_{2\,out} + nCO_{out} + nCH_3OH_{out} + nCH_{4\,out}}\right) \times 100\% \quad (2)$$

CO and CH_3OH selectivity (equation 3-4)

$$S_{(CO)} = \left(\frac{nCO_{out}}{nCO_{out} + nCH_3OH_{out} + nCH_{4\,out}}\right) \times 100\% \quad (3)$$

$$S_{(CH_3OH)} = \left(\frac{nCH_3OH_{out}}{nCO_{out} + nCH_3OH_{out} + nCH_{4\,out}}\right) \times 100\ \% \quad (4)$$

Space time yield (STY) of CO (equation 5):

$$STY_{(CO)} = \left(\frac{SV \times [CO_2] \times X_{(CO_2)} \times S_{(CO)}}{224 \times 3600}\right) \quad (5)$$

Where nCO_{2out}, nCO_{out}, nCH_3OH_{out}, nCH_{4out} are moles of CO_2, CO, CH_3OH and CH_4 calculated from GC analysis. SV is space velocity in mL h^{-1} g^{-1}, $[CO_2]$ is the concentration of CO_2 present in the feed gas mixture in %. STY of CO is reported in μmol g^{-1} s^{-1}.

Acknowledgements

This work was supported by JSPS Grant-in-Aid for Scientific Research (C) KAKENHI JP22K04821.

Conflict of Interest

The authors declare no conflict of interest.

Data availability Statement

The data that support the findings of this study are available from the corresponding author upon reasonable request.

Keywords: CO_2 hydrogenation, reverse water gas shift, redox, mixed oxide, reverse Mars-van Krevelen mechanism

[1] J. Qi, J. Finzel, H. Robatjazi, M. Xu, A. S. Hoffman, S. R. Bare, X. Pan, P. Christopher, *J. Am. Chem. Soc.* **2020**, *142*, 14178–14189.

[2] Y. Li, W. Gao, M. Peng, J. Zhang, J. Sun, Y. Xu, S. Hong, X. Liu, X. Liu, M. Wei, B. Zhang, D. Ma, *Nat. Commun.* **2020**, *11*, 1–8.

[3] S. Lyu, L. Wang, Z. Li, S. Yin, J. Chen, Y. Zhang, J. Li, Y. Wang, *Nat. Commun.* **2020**, *11*, 1–8.

[4] J. Bao, G. Yang, Y. Yoneyama, N. Tsubaki, *ACS Catal.* **2019**, *9*, 3026–3053.

[5] J. Li, Y. He, L. Tan, P. Zhang, X. Peng, A. Oruganti, G. Yang, H. Abe, Y. Wang, N. Tsubaki, *Nat. Catal.* **2018**, *1*, 787–793.

[6] H.-X. Liu, S.-Q. Li, W.-W. Wang, W.-Z. Yu, W.-J. Zhang, C. Ma, C.-J. Jia, *Nat. Commun.* **2022**, *13*, 867.

[7] P. C. Zonetti, S. Letichevsky, A. B. Gaspar, E. F. Sousa-Aguiar, L. G. Appel, *Appl. Catal. A Gen.* **2014**, *475*, 48–54.

[8] Q. Zhang, J. Kang, Y. Wang, *ChemCatChem* **2010**, *2*, 1030–1058.

[9] X. Jiang, X. Nie, X. Guo, C. Song, J. G. Chen, *Chem. Rev.* **2020**, *120*, 7984–8034.

[10] B. Liang, H. Duan, X. Su, X. Chen, Y. Huang, X. Chen, J. J. Delgado, T. Zhang, *Catal. Today* **2017**, *281*, 319–326.

[11] S. Kattel, W. Yu, X. Yang, B. Yan, Y. Huang, W. Wan, P. Liu, J. G. Chen, *Angew. Chemie - Int. Ed.* **2016**, *55*, 7968–7973.

[12] A. Goguet, F. Meunier, J. P. Breen, R. Burch, M. I. Petch, A. Faur Ghenciu, *J. Catal.* **2004**, *226*, 382–392.

[13] S. Mine, T. Yamaguchi, K. W. Ting, Z. Maeno, S. M. A. H. Siddiki, K. Oshima, S. Satokawa, K. I. Shimizu, T. Toyao, *Catal. Sci. Technol.* **2021**, *11*, 4172–4180.

[14] L. Chen, R. R. Unocic, A. S. Hoffman, J. Hong, A. H. Braga, Z. Bao, S. R. Bare, J. Szanyi, *JACS Au* **2021**, *1*, 977–986.

[15] J. Zhu, G. Zhang, W. Li, X. Zhang, F. Ding, C. Song, X. Guo, *ACS Catal.* **2020**, *15*, 57.

[16] A. Parastaev, V. Muravev, E. Huertas Osta, A. J. F. van Hoof, T. F. Kimpel, N. Kosinov, E. J. M. Hensen, *Nat. Catal.* **2020**, *3*, 526–533.

[17] J. Li, Y. Lin, X. Pan, D. Miao, D. Ding, Y. Cui, J. Dong, X. Bao, *ACS Catal.* **2019**, *9*, 6342–6348.

[18] M. Ronda-Lloret, S. Rico-Francés, A. Sepúlveda-Escribano, E. V. Ramos-Fernandez, *Appl. Catal. A Gen.* **2018**, *562*, 28–36.

[19] L. Chen, D. Wu, C. Wang, M. Ji, Z. Wu, *J. Environ. Chem. Eng.* **2021**, *9*, 105183.

[20] G. Zhou, F. Xie, L. Deng, G. Zhang, H. Xie, *Int. J. Hydrogen Energy* **2020**, *45*, 11380–11393.

[21] L. Lin, S. Yao, Z. Liu, F. Zhang, N. Li, D. Vovchok, A. Martínez-Arias, R. Castaneda, J. Lin, S. D. Senanayake, D. Su, D. Ma, J. A. Rodriguez, *J. Phys. Chem. C* **2018**, *122*, 12934–12943.

[22] S. C. Yang, S. H. Pang, T. P. Sulmonetti, W. N. Su, J. F. Lee, B. J. Hwang, C. W. Jones, *ACS Catal.* **2018**, *8*, 12056–12066.

[23] Y. Zhang, L. Liang, Z. Chen, J. Wen, W. Zhong, S. Zou, M. Fu, L. Chen, D. Ye, *Appl. Surf. Sci.* **2020**, *516*, 146035.

[24] C. S. Chen, J. H. Lin, J. H. You, C. R. Chen, *J. Am. Chem. Soc.* **2006**, *128*, 15950–15951.

[25] D. Vovchok, C. Zhang, S. Hwang, L. Jiao, F. Zhang, Z. Liu, S. D. Senanayake, J. A. Rodriguez, *ACS Catal.* **2020**, *10*, 10216–10228.

[26] M. V Twigg, M. S. Spencer, *Appl. Catal. A Gen.* **2001**, *212*, 161–174.

[27] J. Wang, C. Tang, G. Li, Z. Han, Z. Li, H. Liu, F. Cheng, C. Li, *ACS Catal.* **2019**, *9*, 10253–10259.

[28] J. Wang, G. Li, Z. Li, C. Tang, Z. Feng, H. An, H. Liu, T. Liu, C. Li, *Sci. Adv.* **2017**, *3*, 1–11.

[29] L. F. Bobadilla, J. L. Santos, S. Ivanova, J. A. Odriozola, A. Urakawa, *ACS Catal.* **2018**, *8*, 7455–7467.

[30] M. Ziemba, L. Schumacher, C. Hess, *J. Phys. Chem. Lett.* **2021**, *12*, 3749–3754.

[31] J. Sánchez-Marcos, I. M. Ochando, R. E. Galindo, R. Martínez-Morillas, C. Prieto, *Phys. Status Solidi Appl. Mater. Sci.* **2010**, *207*, 1549–1553.

[32] S. Roy, A. Cherevotan, S. C. Peter, *ACS Energy Lett.* **2018**, *3*, 1938–1966.

[33] S. De, A. Dokania, A. Ramirez, J. Gascon, *ACS Catal.* **2020**, *10*, 14147–14185.

[34] S. Kattel, P. Liu, J. G. Chen, *J. Am. Chem. Soc.* **2017**, *139*, 9739–9754.

[35] M. M. J. Li, H. Zou, J. Zheng, T. S. Wu, T. S. Chan, Y. L. Soo, X. P. Wu, X. Q. Gong, T. Chen, K. Roy, G. Held, S. C. E. Tsang, *Angew. Chemie - Int. Ed.* **2020**, *59*, 16039–16046.

[36] G. Liu, H. G. Yang, X. Wang, L. Cheng, H. Lu, L. Wang, G. Q. Lu, H. M. Cheng, *J. Phys. Chem. C* **2009**, *113*, 21784–21788.

[37] X. Chen, L. Liu, P. Y. Yu, S. S. Mao, *Science* **2011**, *331*, 746–750.

[38] H. Liu, H. T. Ma, X. Z. Li, W. Z. Li, M. Wu, X. H. Bao, *Chemosphere* **2003**, *50*, 39–46.

[39] O. Martin, A. J. Martín, C. Mondelli, S. Mitchell, T. F. Segawa, R. Hauert, C. Drouilly, D. Curulla-Ferré, J. Pérez-Ramírez, *Angew. Chemie - Int. Ed.* **2016**, *55*, 6261–6265.

[40] N. H. M. Dostagir, R. Rattanawan, M. Gao, J. Ota, J. Y. Hasegawa, K. Asakura, A. Fukouka, A. Shrotri, *ACS Catal.* **2021**, *11*, 9450–9461.

[41] J. Wang, G. Zhang, J. Zhu, X. Zhang, F. Ding, A. Zhang, X. Guo, C. Song, *ACS Catal.* **2021**, *11*, 1406–1423.

Entry for the Table of Contents

Insert graphic for Table of Contents here.

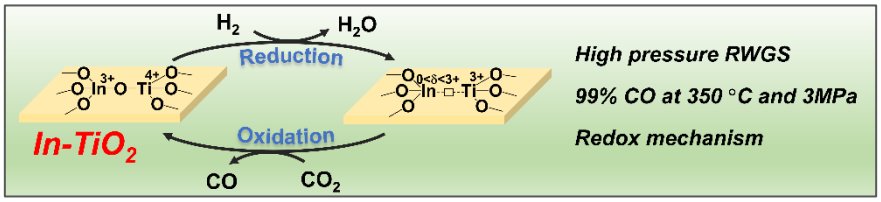

Reverse water gas shift reaction under unfavorable condition of high pressure and low temperature is reported. 99% CO selectivity with high yield was obtained owing to the redox nature of reaction over easily reducible interface of In-TiO_2 mixed oxide.

Institute and/or researcher Twitter usernames: